Atmospheric
Measurement
Techniques

Discussions

1   **TROPOMI Aerosol Products: Evaluation and Observations of**

2   **Synoptic Scale Carbonaceous Aerosol Plumes during 2018-2020**

3   Omar Torres[1], Hiren Jethva[2], Changwoo Ahn[3], Glen Jaross[1], and Diego G. Loyola[4]

4

5   [1] NASA Goddard Space Flight Center, Greenbelt, MD, 20771, USA

6   [2] Universities Space Research Association USRA/GESTAR, Columbia, MD, USA

7   [3] Science Systems and Applications Inc., Lanham, MD USA

8   [4] German Aerospace Center (DLR), Remote Sensing Technology Institute, Oberpfaffenhofen, 82234 Weßling,

9   Germany

10   *Correspondence to* Omar Torres (omar.o.torres@nasa.gov)

11

12   **Abstract.** TROPOMI near-UV radiances are used as input to an inversion algorithm that simultaneously retrieves

13   aerosol optical depth (AOD) and single scattering albedo (SSA) as well as the improved qualitative UV Aerosol

14   Index (UVAI) that accurately accounts for the angular scattering effects of water clouds. We first present the

15   TROPOMI aerosol algorithm (TropOMAER), an adaptation of the currently operational OMI near-UV

16   (OMAERUV & OMACA) inversion schemes, that take advantage of TROPOMI's unprecedented fine spatial

17   resolution at UV wavelengths, and the availability of ancillary aerosol-related information to derive aerosol loading

18   in cloud-free and above-cloud aerosols scenes. An evaluation analysis of TROPOMI-retrieved AOD and SSA

19   products using sun-photometer observations shows improved levels of agreement with respect to those obtained

20   with the heritage coarser resolution sensor. We then use TropOMAER aerosol retrieval results to discuss the US

21   Northwest and British Columbia 2018 wildfire season, the 2019 biomass burning season in the Amazon Basin, and

22   the unprecedented January 2020 fire season in Australia that injected huge amounts of carbonaceous aerosols in the

23   stratosphere.

24

25   **1 Introduction**

26

27   The TROPOspheric Monitoring Instrument (TROPOMI) on the Sentinel-5 Precursor (S5P) satellite launched on

28   October 13, 2017 is the first atmospheric monitoring mission within the European Union Copernicus program. The

29   objective of the mission is the operational monitoring of trace gas concentrations for atmospheric chemistry and

30   climate applications. TROPOMI is the follow-on mission to the successful Aura Ozone Monitoring Instrument

31   (OMI, Levelt et al., 2006) that has been operating since October 2004, the Global Ozone Monitoring Experiment-2

32   (GOME-2, Munro et al., 2016) sensors on the Metop satellites operating since 2006, and previous missions such as

33   SCanning Imaging Absorption SpectroMeter for Atmospheric CHartographY (SCIAMACHY, Bovensmann et al.,

34   1999). The S5P mission precedes the upcoming Sentinel-5 (S5) mission, a TROPOMI-like sensor, and the

35   geostationary Sentinel-4 (S4) mission (Ingmann et al., 2012).

1   TROPOMI is a high spectral resolution spectrometer covering eight spectral windows from the ultraviolet (UV) to

2   the shortwave infrared regions of the electromagnetic spectrum. The instrument operates in a push-broom

3   configuration, with a swath width of about 2600 km on the Earth's surface. The typical pixel size (near nadir) is

4   5.5x3.5 km^2 for all spectral bands, with the exception of the UV1 band (5.5x28 km^2) and SWIR bands (5.5x7 km^2).

5   On ESA's behalf, DLR generates Level 1b radiance data and level 2 products including trace gas (O_3, NO_2, SO_2,

6   CO, CH_4, and CH_2O), aerosols (UV aerosol index and O_2-A band aerosol layer height) and cloud properties. No

7   standard quantitative aerosol products are currently available from TROPOMI. Per NASA-ESA interagency

8   collaboration agreement TROPOMI level 1b calibrated radiance data and level-2 retrieved products, are available at

9   the Goddard Earth Sciences Data and Information Services Center (GES DISC, https://disc.gsfc.nasa.gov/datasets/).

10   In this paper, we report first results of a NASA research aerosol algorithm using TROPOMI observations at near-

11   UV wavelengths. A description of the algorithm is presented in section 2, followed by a detailed evaluation of

12   retrieval results in section3. In section 4, we use TROPOMI derived information to discuss synoptic scale aerosol

13   events taken place in different regions of the world since the launch of TROPOMI in 2017.

14

15   **2 NASA TROPOMI Aerosol Products**

16

17   **2.1 Heritage Algorithm**

18   The NASA OMI aerosol retrieval algorithms for cloud free conditions (OMAERUV, Torres et al., 2007; 2013;

19   2018), and for above-cloud aerosols (OMACA, Torres et al, 2012; Jethva et al., 2018) have been combined into a

20   single algorithm (TropOMAER) and applied to TROPOMI observations. TropOMAER ingests measured

21   TROPOMI radiances at 354 nm and 388 nm to retrieve aerosol optical depth (AOD) and single scattering albedo

22   (SSA) for cloud-free conditions, and above cloud aerosol optical depth (ACAOD) for overcast conditions. Retrievals

23   are carried out at 388 nm and reported also at 354 nm and 500 nm.

24   TropOMAER also produces an improved UV Aerosol Index (UVAI) that accurately accounts for the angular

25   scattering effects of water clouds and thus, reduces the UVAI across-track angular dependence and eliminates

26   spurious non-zero values produced by the previously used LER-based UVAI definition (Torres et al., 2018).

27   As in the heritage OMAERUV algorithm, AIRS observations of carbon monoxide (CO), used as a tracer of

28   carbonaceous aerosols (Torres et al 2013), and a CALIOP-based climatology of aerosol layer height (Torres et al.,

29   2013), are used in TropOMAER for aerosol type identification and aerosol layer height (ALH) determination. Future

30   algorithm enhancement will explore the utilization of TROPOMI retrieved information on ALH and CO, as well as

31   additional available spectral measurements for aerosol typing.

32   TropOMAER uses the ESA-produced VIIRS/SNPP cloud mask re-gridded to the TROPOMI spatial resolution

33   (Siddans, 2016) product for the identification of TROPOMI pixels suitable for aerosol retrieval.

34

35   **2.2 Calibration**

36   In this work, we use the UVIS (UV/Visible) band 3 of TROPOMI level 1b product (Kleipool et al., 2018).

37   TROPOMI version 1 reflectances for band 3 are within 5%-10% compared with OMI and OMPS (Rozemeijer and

1   Kleipool, 2019). It is expected that the upcoming version 2 of the TROPOMI level 1b product will solve

2   inconsistencies of the radiometric calibration detected in the UV and UVVIS spectrometers using in-flight

3   measurements and it will include degradation correction for the affected bands (Ludewig et al., 2020).

4   For this application, we use TROPOMI calibration coefficients at 354 and 388 nm derived using an ice reflectance

5   based vicarious approach that has been historically used in the monitoring of calibration of NASA UV sensors

6   (Jaross and Warner, 2008). A fixed irradiance file was used for the Earth-Sun distance correction. We plan to redo

7   all calibration adjustment and reprocessing when an improved version 2 of the level 1b product is released by ESA.

8

9   **3 Evaluation of TropOMAER Products**

10

11   Evaluation results of TROPOMI-retrieved AOD and SSA albedo using ground-based observations are presented

12   here. A standard satellite-to-ground comparison of measured AOD and SSA was carried out using globally

13   distributed measurements of these parameters by Aerosol Robotic Network (AERONET, Holben et al., 1998).

14   At most AERONET sites AOD at 380 nm is measured, allowing a direct comparison to TROPOMI 388 nm

15   retrievals. However, the AERONET radiance inversion algorithm that retrieves particle size information and

16   complex refractive index, does not retrieve SSA at wavelengths shorter than 440 nm. Therefore, the evaluation of

17   TROPOMI 388 nm SSA retrievals includes the wavelength transformation to 440 nm based on the assumed spectral

18   dependence of absorption in the algorithm (Jethva et al., 2014). Future TROPOMI SSA evaluation work will use

19   measurements from the regional SKYNET network (Nakajima et al., 1996; Hashimoto et al., 2012) that retrieves

20   SSA at 380 nm facilitating the direct comparison to satellite measurements (Jethva, et al., 2019).

21

22   **3.1 AOD Validation**

23

24   AOD comparisons at 388 nm were carried out at several AERONET sites. Ground-based AOD values averaged

25   within ±10 min of the satellite overpass, were compared to spatially averaged TROPOMI retrievals within a 20 km

26   radius of the AERONET site. Resulting scatter plots for the 12 representative sites listed in Table 1 are shown in

27   Figure 1. Calculated correlation coefficients and the parameters of the associated linear fit (y-intercept and slope) are

28   summarized in Table 1, along with number of matchups (N) and the percent of matched points in agreement within

29   30%. The data in Table 1 is listed in decreasing slope value order, to facilitate the discussion.

30   The validation exercise yielded correlation coefficients between 0.79 and 0.94 and root mean square error (RMSE)

31   values lower than 0.20 at 10 out of the selected 12 sites. Slightly larger RMSE values (0.22) were obtained at the

32   Lumbini, Nepal and New Delhi, India locations. Regarding the linear fit results, slope values between 0.75 and 1.25

33   are reported at 9 sites, and between 0.8 and 1.0 at six sites. The comparison yields y-intercept values between 0.15

34   and 0.25 at all sites but New Delhi (0.44). The high y-intercept at all sites in this analysis, is likely the result of a

35   remaining calibration offset and/or the effect of the coarse resolution surface albedo data set currently used in

36   TropOMAER. These issues are currently under investigation.

1   On surface-satellite AOD scatter plots, the effect of sub-pixel cloud contamination in coarse spatial resolution

2   sensors (TOMS, OMI) shows generally an overestimation at AOD's 0.3 and lower [Torres et al., 2002; Ahn et al.,

3   2014]. In the TROPOMI evaluation discussed here, this effect is apparent at sites associated with typically large

4   aerosol loads (notably Mongu, Banizoumbuo, Beijing). At these sites, subpixel cloud contamination effects are

5   observed in TROPOMI retrieved low AOD values. At sites characterized by lower aerosol burden, however, sub-

6   pixel cloud contamination in TROPOMI AOD retrievals is not as obvious as in similar evaluations of OMI retrievals

7   [Ahn et al., 2014]. This apparent improvement in the quality of satellite near UV AOD is likely a result of the

8   combined effect of TROPOMI's finer spatial resolution, and the availability of the collocated VIIIRS cloud mask

9   that allows the identification of pixels suitable for AOD retrievals with minimum cloud presence.

10

11   **3.2 SSA Evaluation**

12

13   In the SSA evaluation, we adopted a spatio-temporal approach to collocate spatially varying TROPOMI SSA

14   retrievals and temporally varying AERONET SSA inversions. The TROPOMI SSA pixels with quality flag '0'

15   (best) were averaged in a grid box of size 0.5 deg. x 0.5 deg. centered at the AERONET station. On the other hand,

16   the AERONET Level-2 SSA data were temporally averaged within ±3 hours of time window centered at the

17   TROPOMI overpass time. The larger temporal window for AERONET allows early morning and late afternoon

18   inversions that are expected to have better accuracy due to larger solar zenith angle and longer atmospheric path

19   length. The spatially and temporally averaged TROPOMI and AERONET SSA data, respectively, then compared as

20   discussed next.

21   Scatter plots of AERONET (x-axis) and TROPOMI (y-axis) 440 nm SSA are shown in Figure 2 for carbonaceous

22   aerosols (left), desert dust particulate (center), and urban-industrial aerosols (right). About 63% (84%) of matched

23   pairs agree within 0.03(0.05) for carbonaceous aerosols. The levels of agreement are 53% (72%) for desert dust, and

24   45% (65%) for urban industrial aerosols. Smaller RMSE (0.036) results from the comparison of carbonaceous

25   particles than those of desert dust and urban industrial aerosols that yield RMSE values of 0.041 and 0.048

26   respectively. Overall, these results are consistent with previous evaluations of OMI retrievals, showing a better

27   agreement with AERONET for carbonaceous particulate.

28

29   **4 Important Aerosol Events**

30

31   **4.1 2018 Fire Season in Northwest USA and Canadian British Columbia**

32

33   The 2018 fire season in the western USA and Canadian British Columbia territory was one of the most active of the

34   last few years. It was estimated that over 8500 fires were responsible for the burning of over 0.8 million hectares

35   which is the largest area burned ever recorded according to California Department of Forestry and Fire Protection

36   (fire.ca.gov) and the National Interagency Fire Center (nfic.gov). From mid-July to August, intense fires in Northern

37   California including the destructive Carr and Mendocino Complex fires, produced elevated smoke layers that drifted

1   east and northeast. In 2018, the British Columbia (B. C) province of Canada encountered its worst fire season on

2   record, surpassing the 2017 record, with more than 2000 wildfires and 1.55 million hectares burned accounting for

3   about 60% of the total burned area in Canada in 2018 (https://www2.gov.bc.ca/gov/content/safety/wildfire-status).

4   Figure 3 shows the spatial extent of the smoke plume generated by wildfires in Canadian B.C. and northwestern

5   USA on August 18, in terms of UVAI, AOD, and SSA products from TROPOMI. The carbonaceous aerosol layers

6   produced by the fires spread over a huge area covering large regions of USA's Midwest and Central Canada. UVAI

7   values as large at 10 associated with above cloud smoke layers can be seen in the Canadian sector of the plume. The

8   height of the aerosol layer oscillated between 3 and 5 km according to CALIOP observations. TROPOMI AOD

9   retrievals show AOD values as high as 3.0, consistent with AERONET ground based observations that, on this day,

10   reported AOD values as large as 1.5 (412 nm) at the Lake Erie site (41.8ºN, 83.2ºW) and values in excess of 3.0 at

11   the Toronto station (43.8ºN, 79.5ºW). Retrieved SSA in the range 0.88-0.92 prevailed over the extended area.

12

13   **4.2 Amazon Basin 2019 Fires**

14

15   Figure 4 shows the spatial distribution of the September 2019 average TROPOMI Aerosol Index, Aerosol Optical

16   Depth, and Aerosol Absorption Optical Depth over the region between the Equator and 40ºS, and between 35ºW and

17   85ºW. Large aerosol concentrations are observed over the southeast

18   Figure 5 shows the time series of monthly average OMI AOD over the region over the last 15 years, and the

19   overlapping TROPOMI AOD observations over the last two years. Seasonal carbonaceous aerosol concentration

20   over the Amazon Basin associated with intense agriculture-related biomass burning has significantly decreased over

21   the last twelve years since 2008. The OMI record shows a remarkable decrease since 2008 when near record high

22   values were observed (Torres et al., 2010). After consecutive AOD September peaks larger than 2.0, in the three-

23   year 2005-2007 period, monthly average AOD over the Amazon basin reduced to values about 0.5. An isolated

24   abrupt increase to larger than 2.0 was again observed in 2010. Since then, the September peak AOD value has

25   remained much lower than 1, except for 2017 and 2019, when September average AOD larger than unity was

26   observed. The 2019 peak AOD value (1.25) was also retrieved by TROPOMI observations.

27   Although the overall regional average was slighter larger than in the previous year, it was about a third of the 2010

28   peak value. As a result of the prevailing regional atmospheric dynamics in 2019, carbonaceous aerosols generated

29   by seasonal biomass burning over region up north were transported towards the southeast reaching large urban

30   centers such as Sao Paulo and Curitiba. This aspect of the 2019 fire season generated lot of media attention.

31

32   **4.3 Australia 2019-2020 Fires**

33

34   The 2019-2020 fire season in Australia resulted in 18.6 million burned hectares, most of them in the New South

35   Wales and Victoria southeastern states (SBS News, 2020). It is estimated tens of people died along with billions of

36   animals that were exterminated including pre-fire near extinction species (Readfearn, 2020). The intense fire activity

37   likely triggered a number of pyroCb's (pyro-cumulonimbus) clouds over a few days between December 30, 2019

1   and early January 2020 injected large amounts of carbonaceous aerosols in the Southern Hemisphere Upper

2   Troposphere – Lower Stratosphere (UTLS). In this section we describe TROPOMI observations of these events in

3   terms of UVAI and AOD retrievals. As observed in visible satellite imagery (not shown) most of the UTLS injected

4   carbonaceous aerosol material was initially above clouds. TROPOMI near UV observations were used in

5   conjunction with aerosol layer height from CALIOP observations as input to a modified version of TropOMAER

6   that handles stratospheric aerosol layers. The retrieved SSA over clear scenes was then used as input in the retrieval

7   of AOD over cloudy pixels (Torres et al., 2012).

8   TROPOMI retrieved AOD was used to produce an estimate of resulting stratospheric aerosol mass (SAM). The

9   SAM calculation procedure involves the separation of the stratospheric AOD component from the total AOD

10   column measurement, and the use of an extinction-to-mass-conversion approximation. This approach was

11   previously applied to EPIC (Earth Panchromatic Imaging Camera) near UV AOD retrievals to calculate the SAM

12   associated with the 2017 British Columbia pyroCb's events (Torres et al., 2020).

13   The identification of stratospheric aerosols is carried out establishing a theoretical relationship between AOD and

14   UVAI for a hypothetical aerosol layer at the tropopause. AOD retrievals associated with UVAI values larger than

15   those indicated by the AOD-UVAI relationship are assumed to correspond to stratospheric aerosols.

16   Figure 6 illustrates the stratospheric aerosol identification method applied to the carbonaceous aerosol layers

17   resulting from the 2017 British Columbia Fires (Torres et al., 2020) on the left and, on the right, from the 2020

18   Australia fires. The solid line illustrates the reference AOD-UVAI relationship.

19   Unlike during the 2017 British Columbia fire episodes, when a large fraction of the pyroCb generated aerosol

20   plume remained initially in the troposphere and some of it ascended diabatically to the stratosphere on the next few

21   days (Torres et al., 2020), during the Australian 2020 pyro-convective fires most of the produced carbonaceous

22   aerosols appear to have gone directly into the stratosphere. Figure 7 shows TROPOMI retrieved UVAI and AOD

23   fields on January 2, 2020. Only small differences in the total column and above-tropopause AOD fields are

24   observed, as most of the aerosol material was directly deposited in the stratosphere.

25   Stratospheric AOD values were converted to mass estimates using the procedure described in Torres et al. (2020)

26   and included Appendix 1 for completeness. Figure 8 shows calculated daily values of aerosol mass (in kilotons)

27   from December 31, 2019 thru January 7, 2020, resulting from aerosols above 12 km, altitude used as a proxy of the

28   tropopause height. Separate aerosol mass retrievals were carried out for cloud free and cloudy scenes, with the daily

29   total SAM given as the sum of these two components. The observed daily monotonic increase from 119 kt on

30   December 31 to 380 kt on January 2 is likely the result of distinct pyroCb events that seemingly injected most of the

31   aerosol mass directly in the stratosphere. Following the January 2 maximum, SAM decreases over the following

32   three days to a minimum of 87 kt on January 5, as a result of dilution processes than spreads the aerosol layer

33   horizontally and thins it out, so that the sensitivity of total mappers is significantly reduced. The sudden increase to

34   166 kt on January 6 is possibly associated with another pyroCb event that injects additional 166 kt. Thus, the

35   TROPOMI-based total SAM estimate is the sum of the two peaks yielding a total of 546 kt, which about twice as

36   much as the estimated SAM for the 2017 British Columbia pyroCb that yielded 268 kt [Torres et al., 2020]. The

Atmospheric
Measurement
Techniques
Discussions

1   uncertainty of the estimated SAM is ±40% which represents the combined effect of uncertainties on assumed

2   aerosol layer height in the AOD retrieval, and the uncertainty in assumed aerosol density (Appendix 1).

3

4   **5 Summary and future work**

5

6   The NASA TropOMAER aerosol algorithm is a modified version of the one applied to OMI observations. Initial

7   retrieval results for the first two years of operation of the TROPOMI sensor were reported. Standard evaluation

8   procedures using ground-based observations were carried out to evaluate the accuracy of TropOMAER retrievals of

9   AOD and SSA at 388 nm. Satellite retrievals of AOD were compared to AERONET observations at 12 locations

10   representative of where carbonaceous aerosols and urban industrial aerosol types are typically present. The

11   validation exercise yielded correlation coefficients between 0.79 and 0.94 and rms values better than 0.20 at 10 out

12   if the 12 sites. Linear fit results show slope values between 0.75 and 1.25 at 9 sites, and between 0.8 and 1.0 at six

13   locations. Reported y-intercept values vary between 0.15 and 0.25 at all sites but New Delhi (0.44). These generally

14   high values are likely due to remaining calibration offsets and/or the effect of the currently used coarse resolution

15   surface albedo data. The initial AERONET-TropOMAER SSA evaluation indicates that nearly 63% (84%) of

16   matched pairs agree within 0.03(0.05) for carbonaceous aerosols, 53% (72%) for desert dust, and 45% (65%) for

17   urban industrial aerosols. These levels of agreement are similar to previous reported evaluation analyses of OMI

18   aerosol retrievals.

19   Three important carbonaceous aerosol events that captured the attention of climate scientists and news media alike.

20   These events, observed by TROPOMI, were briefly described here in terms of TropOMAER products.

21   The atmospheric aerosol load generated by the hundreds of fires in western USA and Southern Canada in the

22   summer of 2018 was measured by both ground-based and spaceborne sensors. The fires-triggered aerosol layers

23   extended over a huge area covering large regions of USA's Midwest and Central Canada. TROPOMI UVAI values

24   as large as 10 produced by above cloud smoke layers were frequently observed. According to CALIOP observations

25   the height of the aerosol layers oscillated between 3 and 5 km. TROMOPI AOD retrievals show AOD values as high

26   as 3.0, consistent with AERONET ground based observations at several sites.

27   After eight years of noticeable reduced biomass burning in Southern Brazil during August and September, a period

28   when agriculture-related biomass burning takes place, numerous fires and, therefore, high levels of carbonaceous

29   aerosols presence were detected in 2019 by both OMI and TROPOMI. As a result of prevailing regional

30   atmospheric dynamics in 2019, carbonaceous aerosols generated by seasonal biomass burning were transported

31   towards the southeast reaching large urban centers. OMI and TROPOMI reported September 2019 monthly and

32   regional average AOD was slightly larger than in the previous year, and about a third of OMI reported 2010 peak

33   (~2.5) value.

34   A number of pyroCb's likely triggered by intense bushfires in the New South Wales province of Australia between

35   December 30, 2019 and early January 2020 injected large amounts of carbonaceous aerosols in the Southern

36   Hemisphere UTLS. Very large values of TROPOMI UVAI observations pointed to an elevated aerosol layer, which

37   was confirmed by CALIOP reports of a distinct high-altitude aerosol layers near 12 km, above tropospheric clouds.

1   TROPOMI retrieved AOD over both cloud-free and cloudy scenes was used to produce an estimate of the injected

2   aerosol mass above 12 km, yielding a total of 546 kt, which is at least twice as much as the estimated carbonaceous

3   aerosol mass injected in the stratosphere by the 2017 Canadian fires. Unlike during the 2017 British Columbia fire

4   episodes, when pyroCb-generated aerosol plume reached the stratosphere in about three days, the 2020 Australian

5   plume seem to have been directly injected into the lower stratosphere.

6   Future TropOMAER algorithm enhancement will explore the utilization of TROPOMI retrieved information on

7   aerosol layer height (Nanda et al., 2019),CO (Martínez-Alonso et al., 2020), clouds (Loyola et al., 2018), geomethry-

8   dependent effective LER (Loyola et al., 2020), as well as taking advantage of additional available spectral

9   measurements for aerosol typing. Work is currently underway on the development of a higher spatial resolution

10   surface albedo data.

11

12   References

13   Ahn, C., O. Torres, and H. Jethva *(2014), Assessment of OMI near-UV aerosol optical depth over land,* J. Geophys.

14   Res. Atmos., 119, 2457–2473, *doi:*10.1002/2013JD020188.

15   Bovensmann, H., Burrows, J. P., Buchwitz, M., Frerick, J., Noël, S., Rozanov, V. V., Chance, K. V., and Goede, A.

16   P. H.: SCIAMACHY: Mission Objectives and Measurement Modes, Journal of the Atmospheric Sciences, 56, 127–

17   150, https://doi.org/10.1175/1520-0469(1999)056%3C0127:SMOAMM%3E2.0.CO;2, 1999.

18   Gassó, S. and Torres, O.: The role of cloud contamination, aerosol layer height and aerosol model in the assessment

19   of the OMI near-UV retrievals over the ocean, Atmos. Meas. Tech., 9, 3031-3052, doi:10.5194/amt-9-3031-2016,

20   2016.

21   Genkova, I., Robaidek, J., Roebling, R., Sneep, M., and Veefkind, P.: Temporal co-registration for TROPOMI cloud

22   clearing, Atmos. Meas. Tech., 5, 595–602, https://doi.org/10.5194/amt-5-595-2012, 2012.

23   Hashimoto, M., Nakajima, T., Dubovik, O., Campanelli, M., Che, H., Khatri, P., Takamura, T., and Pandithurai, G.:

24   Development of a new data-processing method for SKYNET sky radiometer observations, Atmos. Meas. Tech., 5,

25   2723–2737, https://doi.org/10.5194/amt-5-2723-2012, 2012

26   van de Hulst, H. C., Light Scattering by Small Particles, chapter 6, New York, Dover Publications, Inc., 1957.

27   Ingmann, P., Veihelmann, B., Langen, J., Lamarre, D., Stark, H., and Courrèges-Lacoste, G. B.: Requirements for

28   the GMES Atmosphere Service and ESA's implementation concept: Sentinels-4/-5 and -5p, REMOTE SENS

29   ENVIRON, 120, 58 – 69, https://doi.org/https://doi.org/10.1016/j.rse.2012.01.023, 2012

30   Jaross, G., and J. Warner (2008), Use of Antarctica for validating reflected solar radiation measured by satellite

31   sensors, J. Geophys. Res., 113, D16S34, doi:10.1029/2007JD008835.

32   Jethva, H., Torres, O., and Ahn, C.: A 12-year long global record of optical depth of absorbing aerosols above the

33   clouds derived from the OMI/OMACA algorithm, Atmos. Meas. Tech., 11, 5837-5864, https://doi.org/10.5194/amt-

34   11-5837-2018, 2018.

35   Jethva, H., O. Torres, and C. Ahn (2014), Global assessment of OMI aerosol single-scattering albedo using ground-

36   based AERONET inversion, J. Geophys. Res. Atmos., 119, doi:10.1002/2014JD021672.

1   Kleipool, Q., Ludewig, A., Babic, L., Bartstra, R., Braak, R., Dierssen, W., Dewitte, P.-J., Kenter, P., Landzaat, R.,
2   Leloux, J., Loots, E., Meijering, P., van der Plas, E., Rozemeijer, N., Schepers, D., Schiavini, D., Smeets, J.,
3   Vacanti, G., Vonk, F., and Veefkind, P.: Prelaunch calibration results of the TROPOMI payload on-board the
4   Sentinel-5 Precursor satellite, Atmos. Meas. Tech., 11, 6439–6479, https://doi.org/10.5194/amt-11-6439-2018,
5   https://www.atmos-meas-tech.net/11/6439/2018/, 2018.
6   Krotkov, N.A., O. Torres, C. Seftor, A.J. Krueger, A. Konstinski, W.I. Rose, G.J.S. Bluth, D. Schneider and S.J.
7   Schaefer, Comparison of TOMS and AVHRR Volcanic Ash Retrievals from the August 1992 Eruption of Mt Spurr,
8   *Geophys. Res. Let*., 26, 455-458, 1999
9   Levelt, P. F., van den Oord, G. H., Dobber, M. R., Malkki, A., Visser, H., de Vries, J., Stammes, P., Lundell, J. O.,
10   and Saari, H.: The ozone monitoring instrument, IEEE Transactions on Geoscience and Remote Sensing, 44, 1093–
11   1101, https://doi.org/10.1109/TGRS.2006.872333, 2006.
12   Loyola, D. G., Xu, J., Heue, K.-P., and Zimmer, W.: Applying FP_ILM to the retrieval of geometry-dependent
13   effective Lambertian equivalent reflectivity (GE_LER) daily maps from UVN satellite measurements, Atmos. Meas.
14   Tech., 13, 985–999, https://doi.org/10.5194/amt-13-985-2020, 2020.
15   Loyola, D. G., Gimeno García, S., Lutz, R., Argyrouli, A., Romahn, F., Spurr, R. J. D., Pedergnana, M., Doicu, A.,
16   Molina García, V., and Schüssler, O.: The operational cloud retrieval algorithms from TROPOMI on board Sentinel-
17   5 Precursor, Atmos. Meas. Tech., 11, 409–427, https://doi.org/10.5194/amt-11-409-2018, 2018.
18   Ludewig, A., Kleipool, Q., Bartstra, R., Landzaat, R., Leloux, J., Loots, E., Meijering, P., van der Plas, E.,
19   Rozemeijer, N., Vonk, F., and Veefkind, P.: In-flight calibration results of the TROPOMI payload on-board
20   theSentinel-5 Precursor satellite, Atmos. Meas. Tech. Discuss., https://doi.org/10.5194/amt-2019-488, in review,
21   2020.
22   Martínez-Alonso, S., Deeter, M., Worden, H., Borsdorff, T., Aben, I., Commane, R., Daube, B., Francis, G., George,
23   M., Landgraf, J., Mao, D., McKain, K., and Wofsy, S.: 1.5 years of TROPOMI CO measurements: Comparisons to
24   MOPITT and ATom, Atmos. Meas. Tech. Discuss., https://doi.org/10.5194/amt-2020-63, in review, 2020.Munro,
25   R., Lang, R., Klaes, D., Poli, G., Retscher, C., Lindstrot, R., Huckle, R., Lacan, A., Grzegorski, M., Holdak, A.,
26   Kokhanovsky, A., Livschitz, J., and Eisinger, M.: The GOME-2 instrument on the Metop series of satellites:
27   instrument design, calibration, and level 1 data processing – an overview, Atmos. Meas. Tech., 9, 1279–1301,
28   https://doi.org/10.5194/amt-9-1279-2016, 2016.
29   Nakajima, T., Tonna, G., Rao, R., Boi, P., Kaufman, Y., and Holben, B.: Use of sky brightness measurements from
30   ground for remote sensing of particulate polydispersions, Appl. Optics, 35, 15, 2672–2686, 1996.
31   Nanda, S., de Graaf, M., Veefkind, J. P., Sneep, M., ter Linden, M., Sun, J., and Levelt, P. F.: Validating TROPOMI
32   aerosol layer height retrievals with CALIOP data, Atmos. Meas. Tech. Discuss., https://doi.org/10.5194/amt-2019-
33   348, in review, 2019.
34   Readfearn, G., 2020, *Silent death: Australia's bushfires push countless species to extinction"*, Guardian Australia, *3*
35   *January 2020.*

1   Reid, J. S., Koppmann, R., Eck, T. F., and Eleuterio, D. P.: A review of biomass burning emissions part II: intensive

2   physical properties of biomass burning particles, Atmos. Chem. Phys., 5, 799-825, https://doi.org/10.5194/acp-5-

3   799-2005, 2005.

4   Rozemeijer, N. C. and Kleipool, Q.: S5P Level 1b Product Readme File, S5P-MPC-KNMI-PRF-L1B, available at:

5   https://sentinel.esa.int/web/sentinel/technical-guides/sentinel-5p/products-algorithms and

6   http://www.tropomi.eu/documents/level-0-1b (last access: 26 March 2020), 2019.

7   SBS News,2020, The numbers behind Australia's catastropic bushfire season, SBS News. 5 January 2020.

8   Siddans, R., S5P-NPP Cloud Processor ATBD, S5P-NPPCRAL-ATBD-0001, available at:

9   https://sentinel.esa.int/web/sentinel/technical-guides/sentinel-5p/products-algorithms and

10 http://www.tropomi.eu/documents/atbd, (last access: 26 March 2020), 2016

11 Torres, O., Bhartia, P. K., Taha, G., Jethva, H., Das, S., Colarco, P., et al (2020). Stratospheric Injection of Massive

12 Smoke Plume from Canadian Boreal Fires in 2017 as seen by DSCOVR-EPIC, CALIOP and OMPS-LP

13 Observations. *Journal of Geophysical Research: Atmospheres*, 125, e2020JD032579.

14 https://doi.org/10.1029/2020JD032579

15 Torres, O., Bhartia, P. K., Jethva, H., and Ahn, C.: Impact of the ozone monitoring instrument row anomaly on the

16 long-term record of aerosol products, Atmos. Meas. Tech., 11, 2701-2715, https://doi.org/10.5194/amt-11-2701-

17 2018, 2018.

18 Torres, O., Ahn, C., and Chen, Z.: Improvements to the OMI near UV aerosol algorithm using A-train CALIOP and

19 AIRS observations, Atmos. Meas. Tech., 6, 3257-3270, doi:10.5194/amt-6-3258-2013, 2013

20 Torres, O, H. Jethva, and P.K. Bhartia, Retrieval of Aerosol Optical Depth above Clouds from OMI Observations:

21 Sensitivity Analysis and Case Studies, Journal. Atm. Sci., 69, 1037-1053, doi:10.1175/JAS-D-11-0130.1, 2012

22 Torres, O., A. Tanskanen, B. Veihelman, C. Ahn, R. Braak, P. K. Bhartia, P. Veefkind, and P. Levelt, Aerosols and

23 Surface UV Products from OMI Observations: An Overview, , *J. Geophys. Res.,* 112, D24S47,

24 doi:10.1029/2007JD008809, 2007

25

1

Site (country)	Lat., Lon.	N	Corr.coef	y-int	Slope	RMSE	Q30%
Hohenpeissenberg (Germany)	47.8N, 11.0E	78	0.81	0.15	1.21	0.09	17
GSFC (USA)	39.0N, 76.8W	50	0.80	0.19	0.99	0.11	22
Lille (France)	50.6N, 3.1E	47	0.88	0.20	0.97	0.09	17
Beijing-CAMS (China)	39.9N, 116.3E	53	0.94	0.23	0.92	0.18	53
Thessaloniki (Greece)	40.6N, 23.0E	103	0.79	0.19	0.84	0.09	41
Fukuoka (Japan)	33.5N, 130.5E	52	0.84	0.16	0.83	0.10	60
Banizoumbou (Niger)	13.5N, 2.7E	111	0.81	0.23	0.81	0.19	54
Mongu (Zambia)	15.3S, 23.3E	122	0.91	0.25	0.76	0.12	43
Leipzig (Germany)	51.4N,12.4E	40	0.81	0.27	0.75	0.11	23
Lumbini (Nepal)	27.5N 83.3E	67	0.85	0.19	0.69	0.22	73
Yonsei_univ (S. Korea)	37.6N, 126.9E	90	0.85	0.25	0.62	0.14	56
New Delhi (India)	28.6N, 77.2E	42	0.79	0.44	0.59	0.22	76

2

3   **Table 1: Summary of linear fit results between AERONET measured and TROPOMI retrieved AOD at 12**
4   **locations. Third column is the number of matchups, columns fourth to six (Q30%) indicates the number of**
5   **(in percent) retrievals in agreement within 30% with the ground-truth observations.**
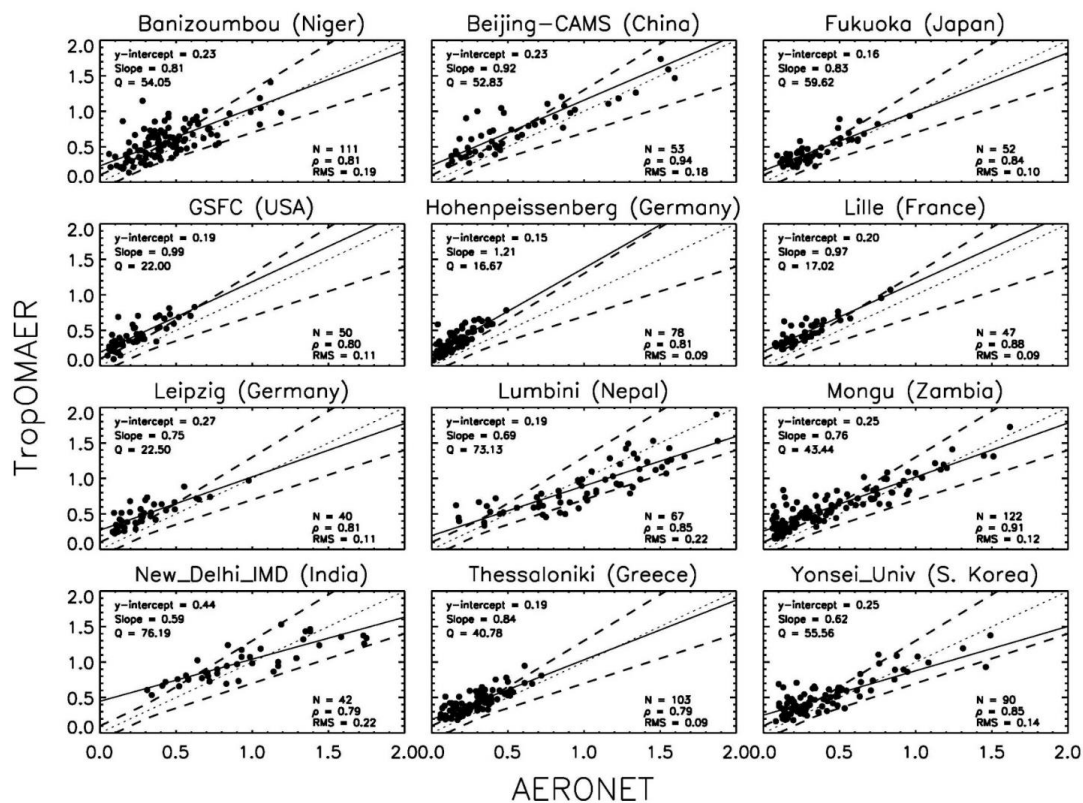
1

2   **Figure 1: Comparison of TROPOMI AOD to AERONET observations at diverse locations around the world.**
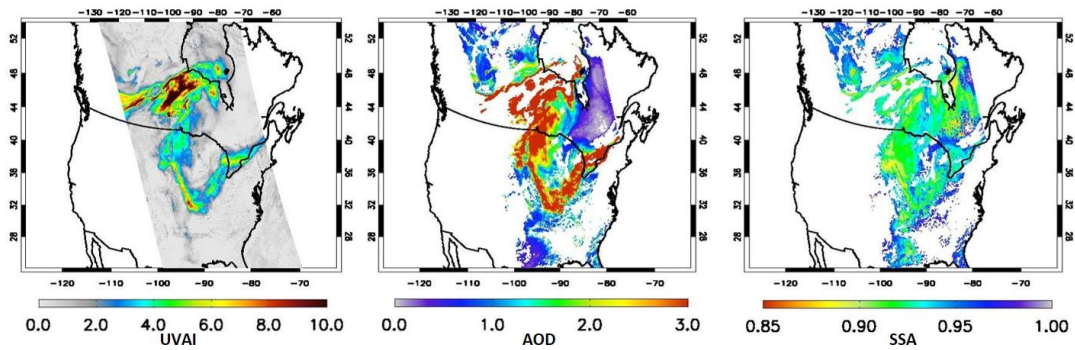
3
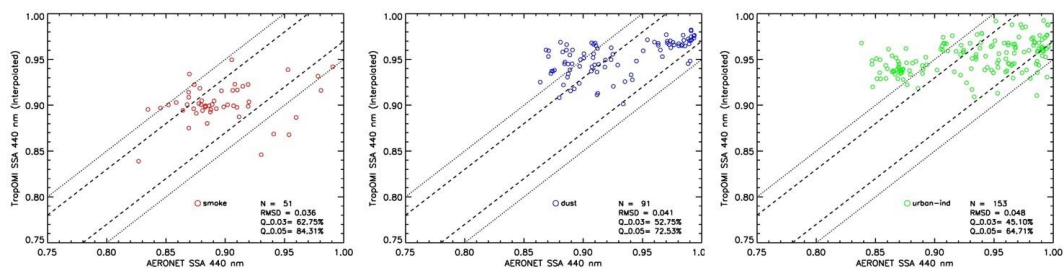
1

2   **Figure 2: TROPOMI Single Scattering Albedo comparison to AERONET observations.**
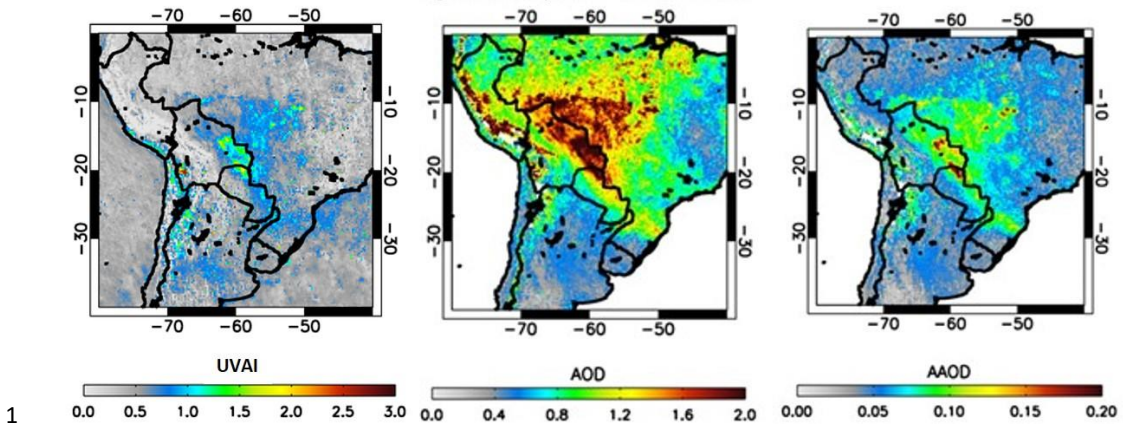
3

1

2   **Figure 3: TROPOMI UV Aerosol Index (left), Aerosol Optical Depth (center), and Aerosol Single Scattering**

3   **Albedo (right) for carbonaceous aerosol plume during California fires on August 18, 2018.**
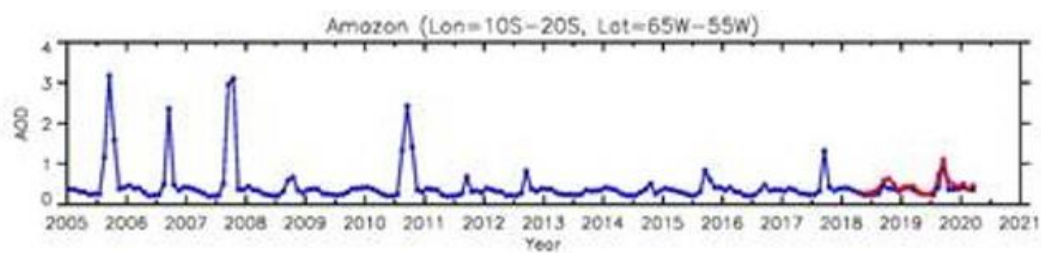
4

5

Figure 4. September 2019 average TROPOMI UV Aerosol Index (left), Aerosol Optical Depth (center), and Aerosol Absorption Optical Depth (right) for carbonaceous aerosols over the Amazon Basin.
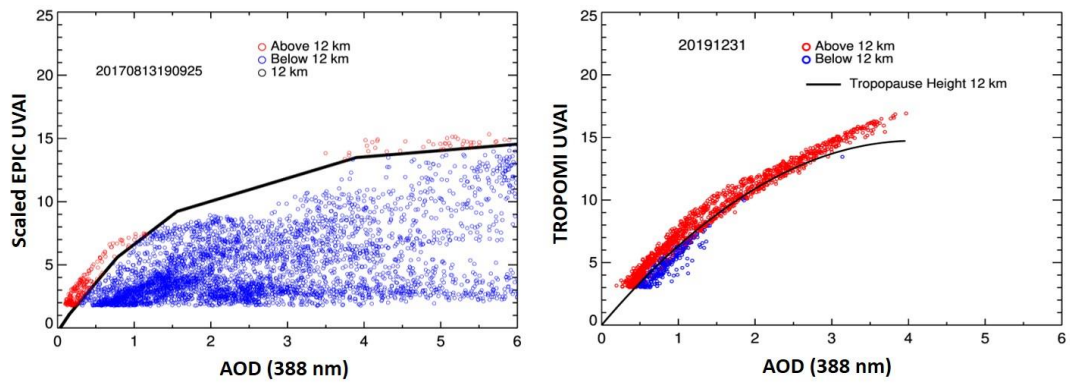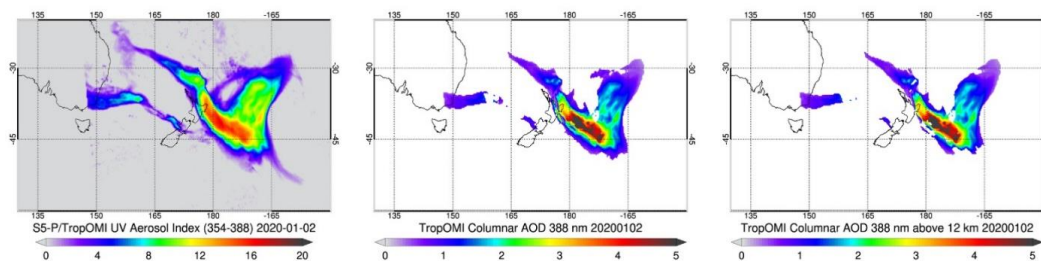
1

2 **Figure 5: Time series of AOD over the amazon basin from OMI (black line) and TROPOMI observations.**
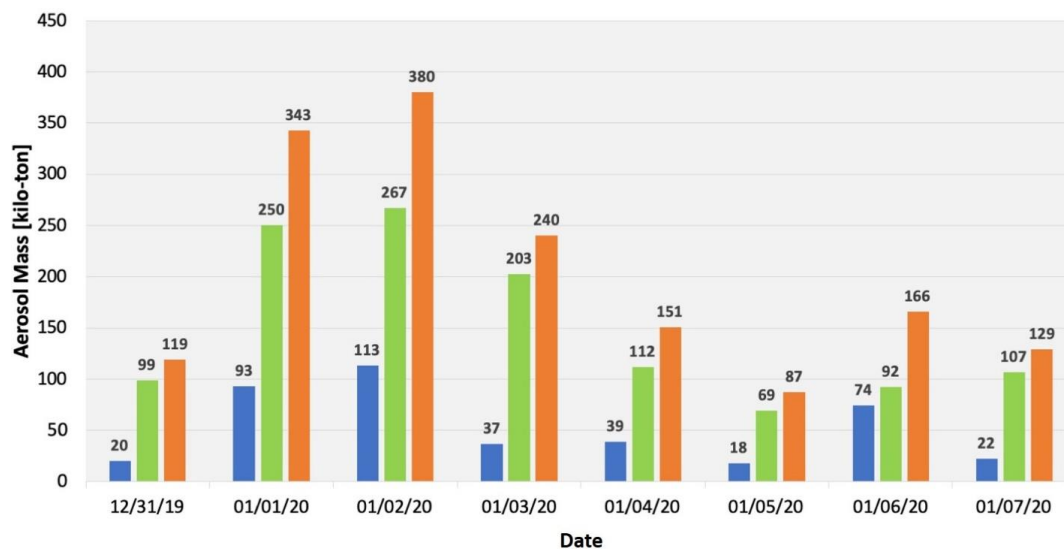
3

1

2   **Figure 6: Comparison of UVAI-AOD relationship for the 2017 Canadian fires (left) and 2020 Australian fires**

3   **(right).**

1

2 **Figure 7. TROPOMI UVAI (left), total column AOD (center) and above 12 km AOD (right) fields of**
3 **Australian smoke plume on January 2, 2020.**

1

2   **Figure 8. Injected aerosol mass in the stratosphere from TROPOMI observations.**

3

Atmospheric
Measurement
Techniques
Discussions

Open Access

EGU

1

2   **Appendix A**

3   **Extinction to mass conversion**

4   The total aerosol mass injected in the stratosphere, M, can be estimated by converting stratospheric AOD (τ_{str}, see
5   below) into an equivalent aerosol mass per unit area, using the equation (Krotkov et al., 1999)

6
$$M = \Sigma \frac{4}{3} \rho r_{eff} A \tau_{str} f\left(r_{eff}\right) \qquad (A\text{-}1)$$

7   that yields the summation of the aerosol mass over the total area covered by the aerosol plume. In Equation A-1, ρ is
8   the aerosol particle mass density in g-cm^{-3}, r_{eff} is the effective radius (μm) associated with the particle size
9   distribution (van de Hulst, 1957), A is the effective geographical area in km^2, associated with retrieved
10   stratospheric AOD, and $f(r_{eff})$ is a dimensionless extinction-to-mass conversion factor, averaging over particle size
11   distribution, defined as

12

13
$$f = \int_0^\infty r^2 n(r)\partial r \Big/ \int_0^\infty r^2 Q_{ext}(r) n(r)\partial r \quad (A\text{-}2)$$

14

15   where $n(r)dr$ is the assumed number particle size distribution and $Q_{ext}(r)$ is the extinction efficiency factor
16   calculated using Mie theory. Calculations were carried out for particle mass density values of 0.79 and 1.53 g-cm^{-3}
17   which cover the range of values reported in the literature (Reid et al., 2005).

18